Electronic Supplementary Material (ESI) for CrystEngComm.

Supporting Information

High-Energy Organic Groups Induced Spectrally Pure Upconversion Emission for Zirconate-/hafnate-Containing Nanocrystals

Xianghong He,[†,‡] Bing Yan*,[†]

[†]Department of Chemistry, Tongji University, Shanghai, 200092, China

[‡]School of Chemistry and Environmental Engineering, Jiangsu University of Technology, Changzhou, 213001, China

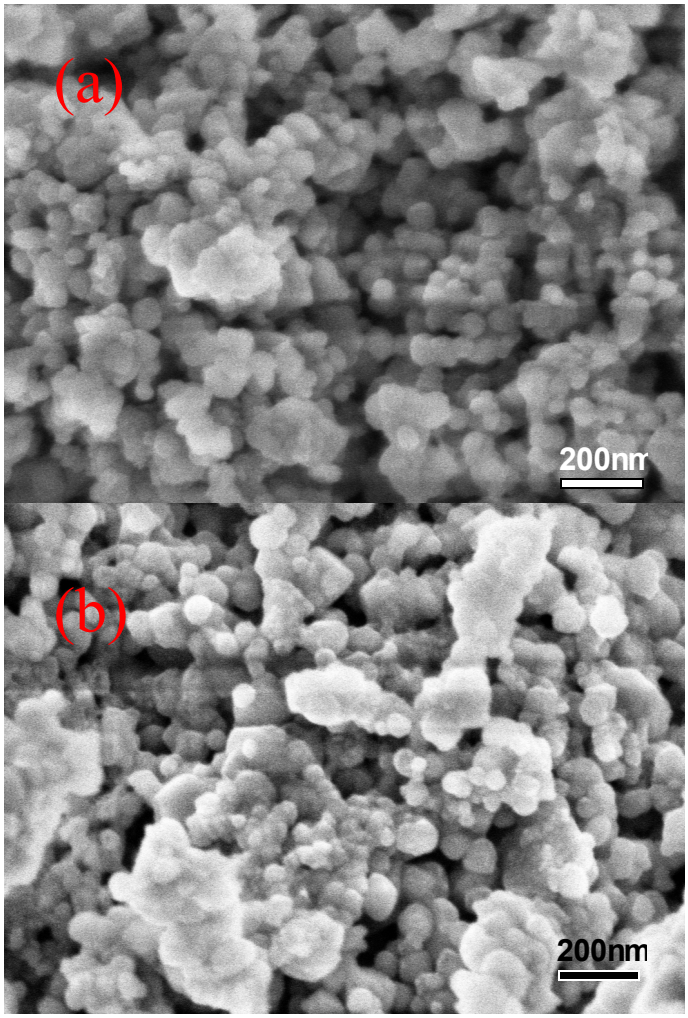

Figure S1 SEM images of as-obtained K_3ZrF_7 (a) and K_3HfF_7 (b) NCs.

Phase and compositional analyses of Yb^{3+}/Er^{3+}-codoped $K_3(Zr,Hf)F_7$ nanophosphors

XRD results of K_3ZrF_7:Yb^{3+},Er^{3+} samples with different concentrations of Yb^{3+} and/or Er^{3+} (panel a of Figure S2, and Figure S3) verify that the cubic K_3ZrF_7 structure is retained even as Yb^{3+} doping content reaches as high as 40 mol%. Compositional analyses of K_3ZrF_7:Yb^{3+},Er^{3+}(x/2 mol%, 5 mol% ≤ x ≤ 40 mol%) and $K_3(Zr_{0.78-t}Hf_t)F_7$:Yb^{3+},Er^{3+}(20/2 mol%, 0.28 ≤ t ≤ 0.78) samples using energy dispersive X-ray spectroscopy (EDS) (Figures S4 and S5) confirm that the chemical signatures taken within different parts of the sample are identical within experimental accuracy and that the as-obtained samples contain K, Zr/Hf, F, Yb, and Er elements. In addition, the actual atomic ratios of these elements were consistent with the designed nominal stoichiometry in each case. With increasing of Yb^{3+} doping level, the diffraction peaks shifted gradually towards the low-angle direction (panel b of Figure S2), which can be attributed to the substitution of Zr^{4+} with an ionic radius of 0.78 Å by Yb^{3+} with a larger ionic radius of 0.93 Å under seven F^- coordination environment.[S01] Figure S6 revealed the XRD patterns $K_3(Zr_{0.78-t}Hf_t)F_7$:Yb^{3+},Er^{3+}(20/2 mol%) samples. Since Hf^{4+} and Zr^{4+} own close ionic radii (0.76 and 0.78 Å for Hf^{4+} and Zr^{4+}, respectively), the products also remained single phase in the case of various contents of Hf^{4+}.

Ref. [S01] D. Q. Chen, L. Lei, R. Zhang, A. P. Yang, J. Xu and Y. S. Wang, Intrinsic single-band upconversion emission in colloidal Yb/Er(Tm):$Na_3Zr(Hf)F_7$ nanocrystals, Chem. Commun., 2012, 48, 10630–10632.

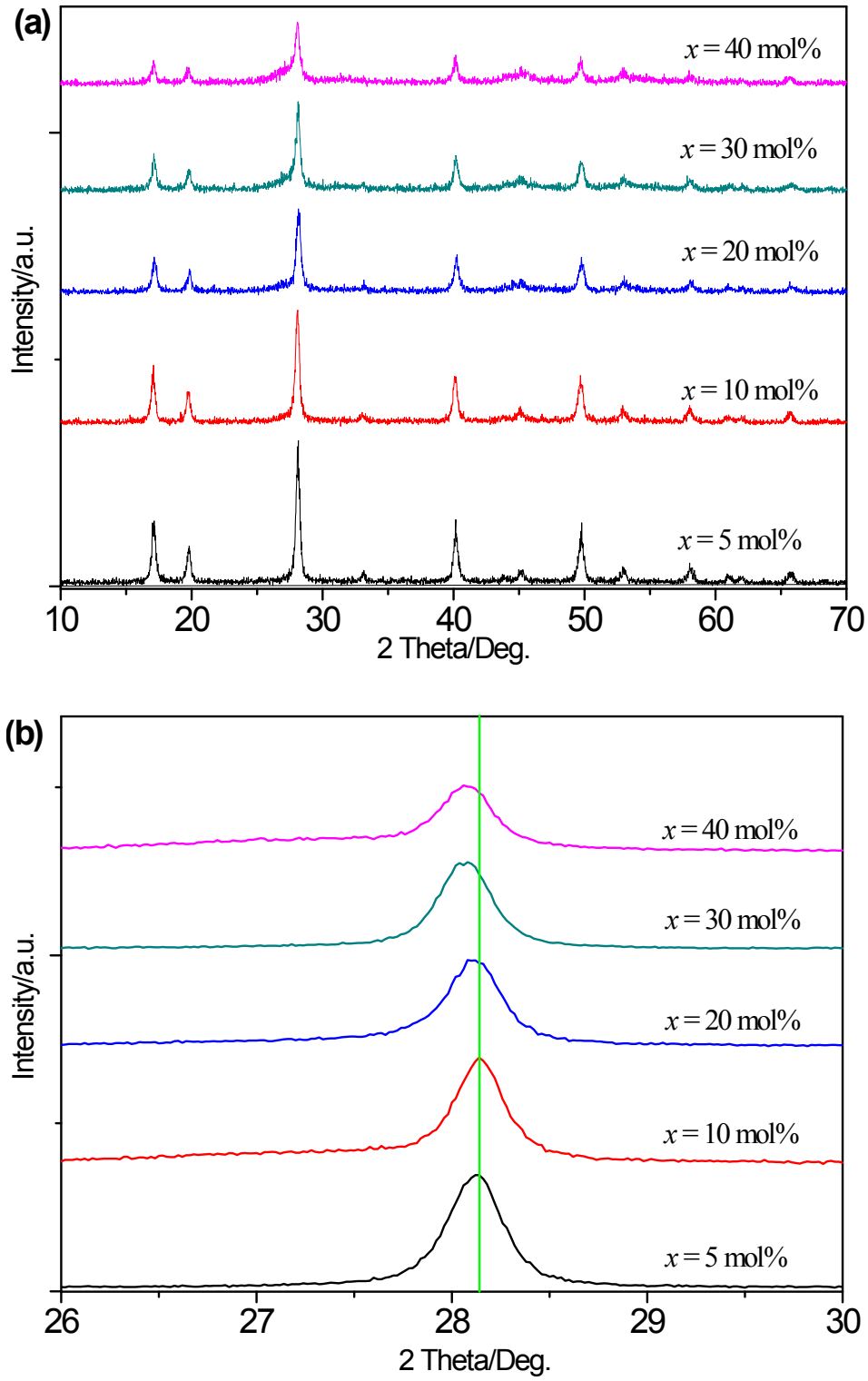

Figure S2 (a) XRD patterns in the 2θ range from 10° to 70° , and (b) XRD patterns in the 2θ range from 26° to 30° of K_3ZrF_7:Yb^{3+},Er^{3+}(x/2 mol%) samples with different concentrations of Yb^{3+} (x value).

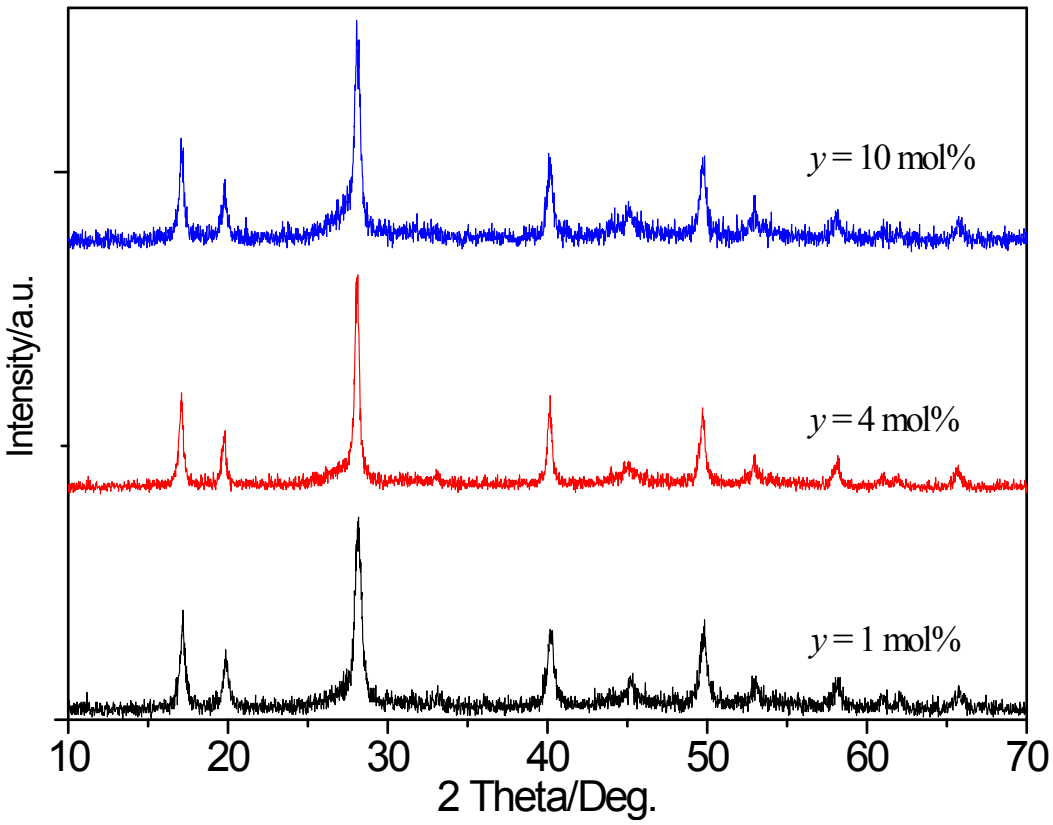

Figure S3 XRD patterns of K_3ZrF_7:Yb^{3+},Er^{3+}(20/y mol%) samples with different doping contents of Er^{3+}(y value).

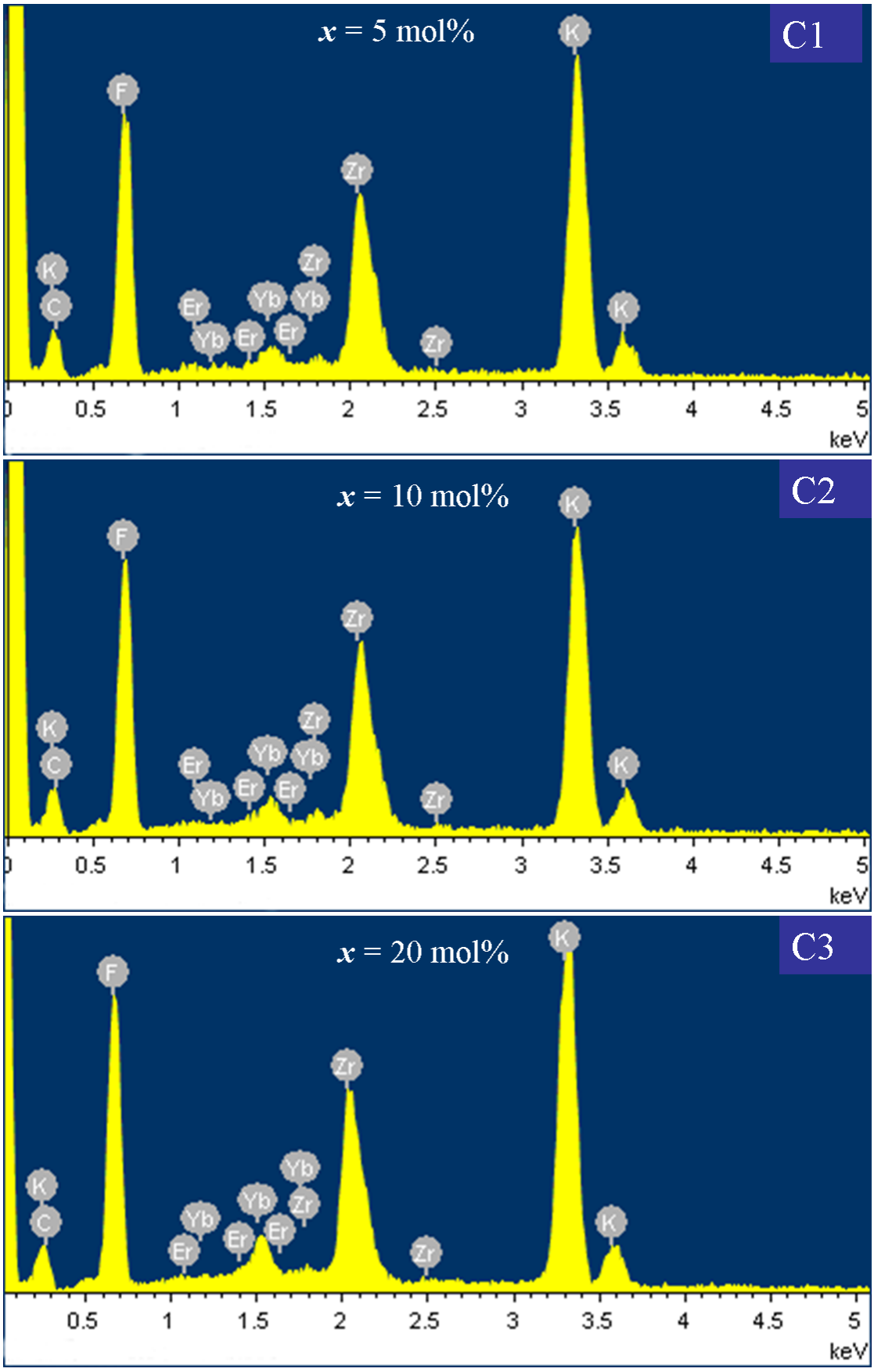
x = 5 mol%
C1
F
K
Zr
K
C
Er
Yb
Yb
Er
Er
Yb
Zr
Zr
K
0
0.5
1
1.5
2
2.5
3
3.5
4
4.5
5
keV
x = 10 mol%
C2
F
K
Zr
K
C
Er
Yb
Yb
Er
Er
Yb
Zr
Zr
K
0
0.5
1
1.5
2
2.5
3
3.5
4
4.5
5
keV
x = 20 mol%
C3
F
K
Zr
K
C
Er
Yb
Yb
Er
Er
Yb
Zr
Zr
K
0.5
1
1.5
2
2.5
3
3.5
4
4.5
5
keV

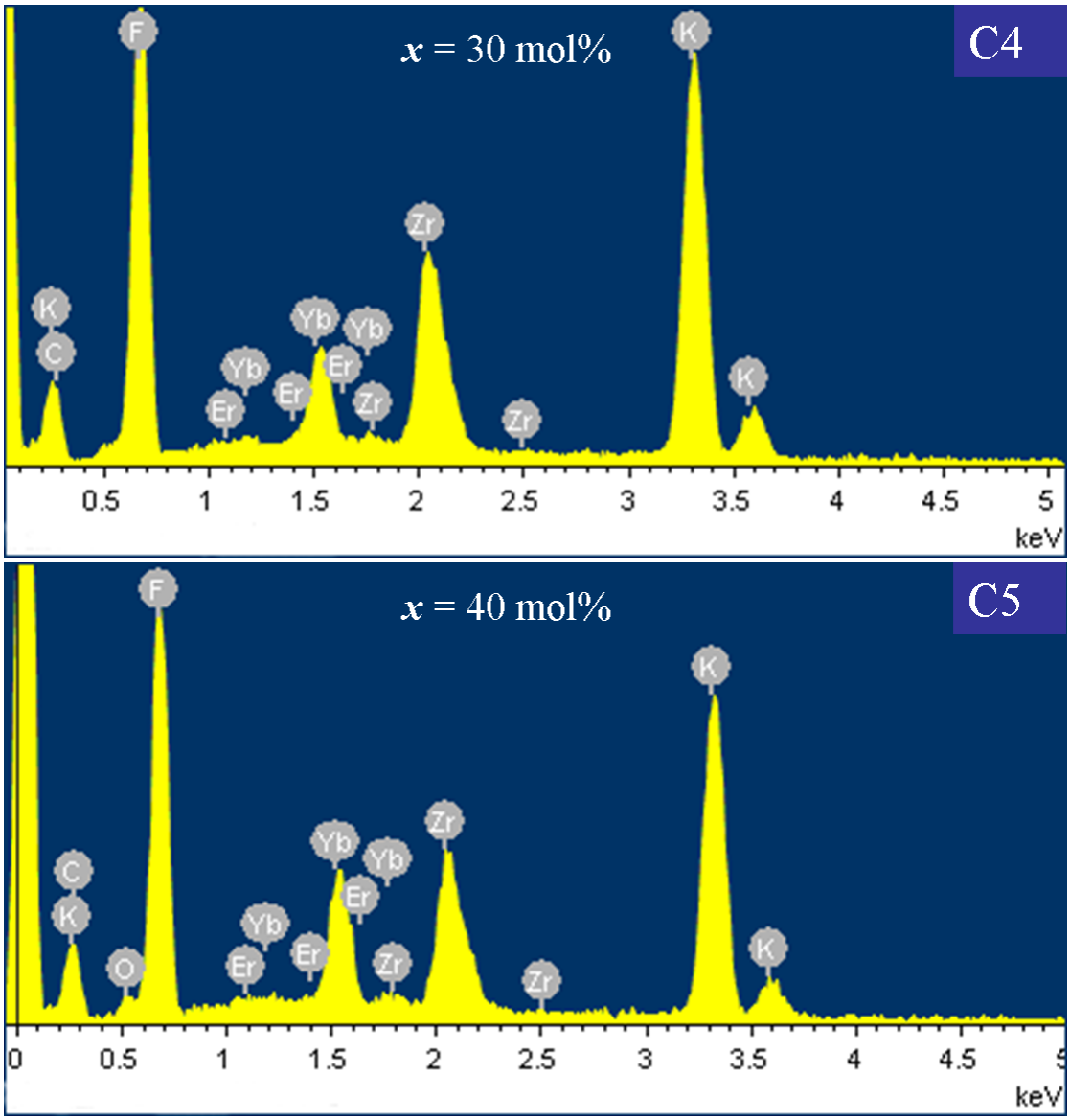

Figure S4 EDS patterns of K_3ZrF_7:Yb^{3+},Er^{3+}(x/2 mol%) samples with different concentrations of Yb^{3+} (x value).

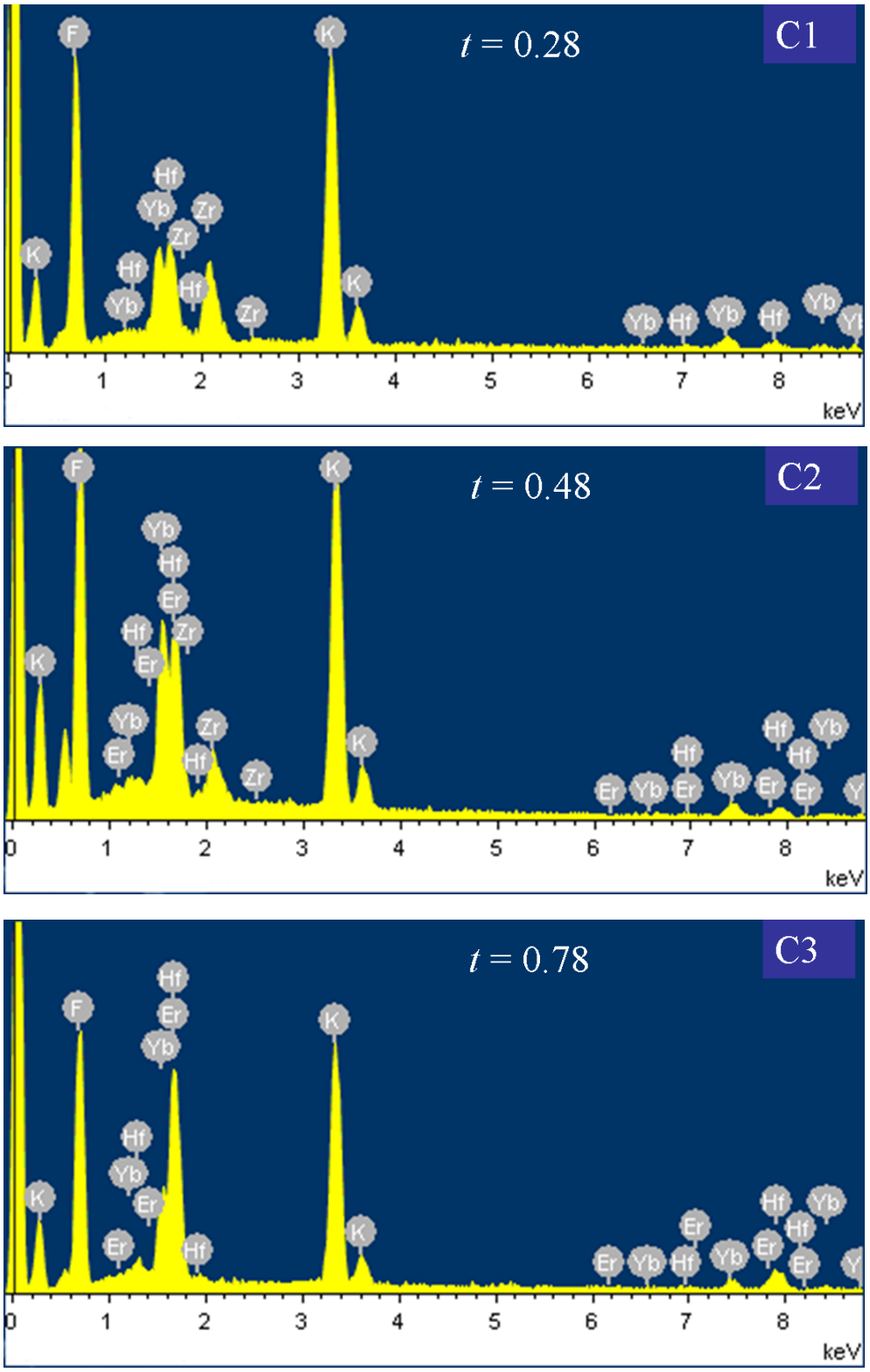

Figure S5 EDS patterns of $K_3(Zr_{0.78-t}Hf_t)F_7$:Yb^{3+},Er^{3+}(20/2 mol%) samples with various contents of Hf^{4+} (t value).

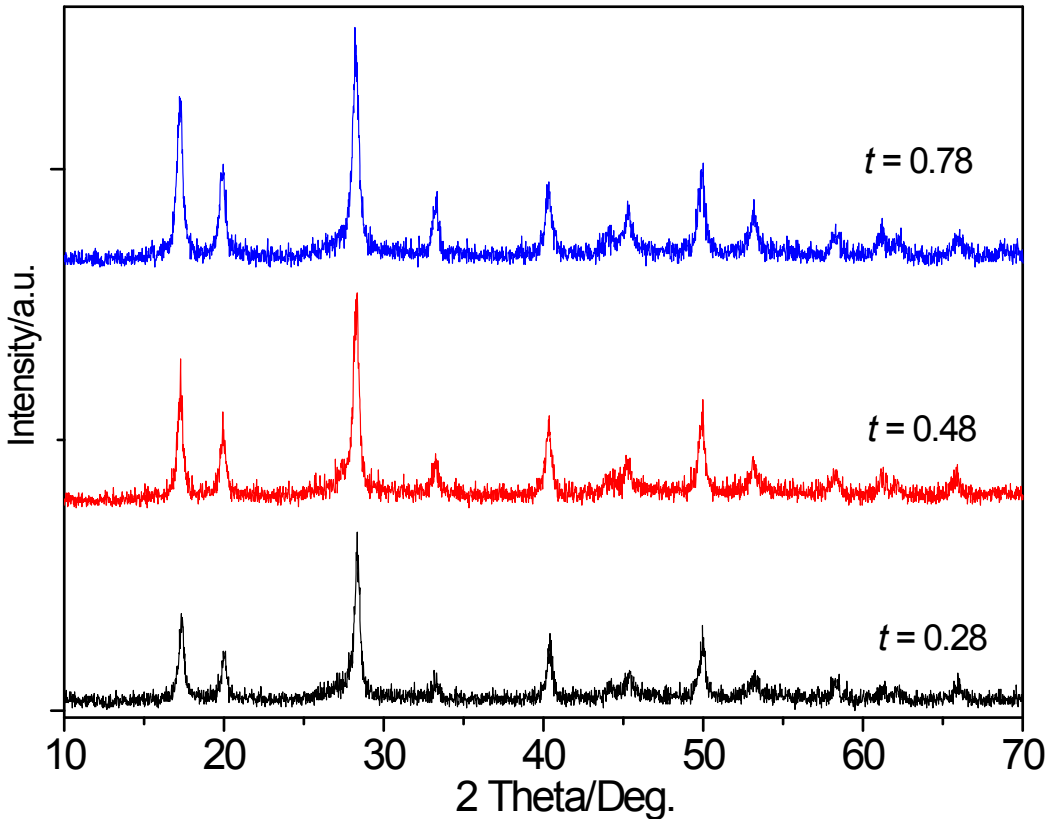

Figure S6 XRD patterns of $K_3(Zr_{0.78-t}Hf_t)F_7:Yb^{3+},Er^{3+}$(20/2 mol%) samples with various contents of Hf^{4+} (t value).

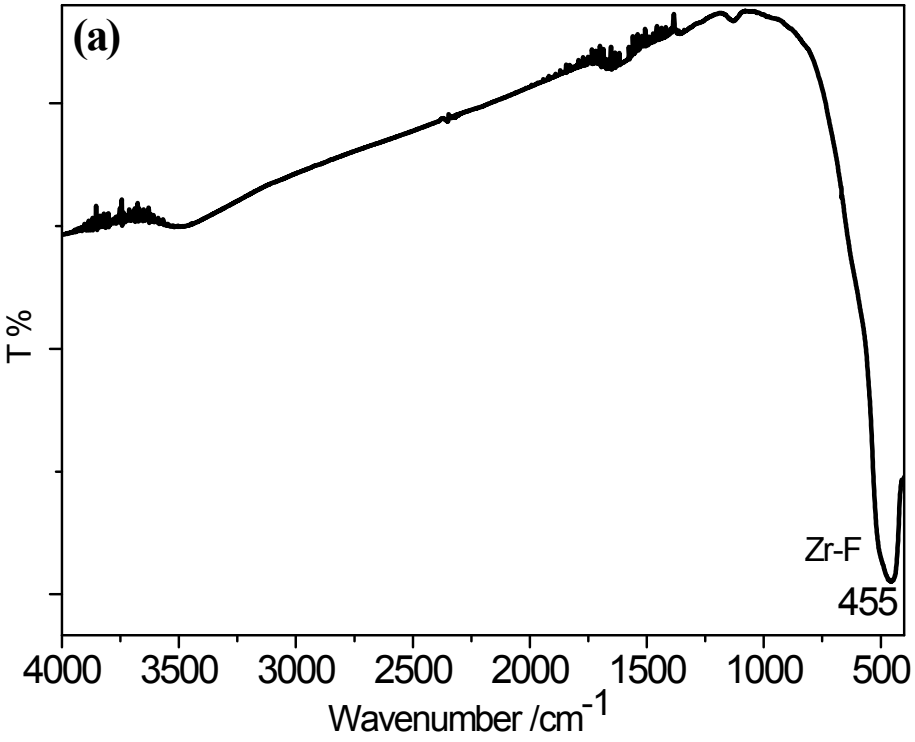

Figure S7 FT-IR spectrum of K_3ZrF_7:Yb^{3+},Er^{3+}(20/2 mol%) sample annealed at 350 ℃.

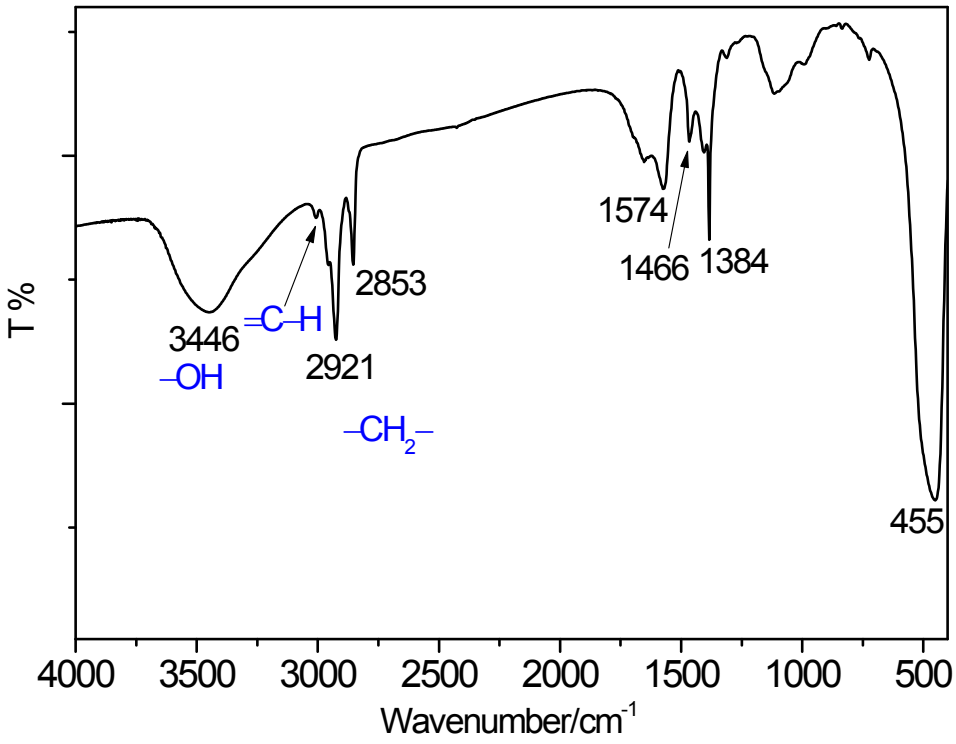

Figure S8 FT-IR spectrum of K_3ZrF_7:Yb^{3+},Er^{3+} NCs.